JACS
JOURNAL OF THE AMERICAN CHEMICAL SOCIETY
Communication
pubs.acs.org/JACS

Dynamic and Reversible Fluorescence Imaging of Superoxide Anion Fluctuations in Live Cells and in Vivo

Wen Zhang,[†] Ping Li,[†] Fan Yang, Xiufen Hu, Chuanzhi Sun, Wei Zhang, Dezhan Chen, and Bo Tang*

College of Chemistry, Chemical Engineering and Materials Science, Engineering Research Center of Pesticide and Medicine Intermediate Clean Production, Ministry of Education, Key Laboratory of Molecular and Nano Probes, Ministry of Education, Shandong Normal University, Jinan 250014, P.R. China

Supporting Information

ABSTRACT: Overgeneration of reactive oxygen species (ROS) is closely associated with cellular damage and diseases. As superoxide anion ($O_2^{\bullet-}$) is the precursor of other ROS, exploring $O_2^{\bullet-}$ fluctuations in cells and in vivo is of great significance. To address this critical need, we have developed a novel reversible fluorescent probe with one-photon and two-photon fluorescence properties, which is well suited for monitoring $O_2^{\bullet-}$ fluxes selectively and dynamically. Imaging results substantiate dynamic and reversible fluorescence responses of this probe to intracellular $O_2^{\bullet-}$ under apoptotic stimuli. Moreover, this probe can conveniently visualize changes in $O_2^{\bullet-}$ concentration during reperfusion injury in hepatocytes, zebrafish, and mice, by means of one-photon or two-photon imaging according to depths of various samples. The present study provides a powerful fluorescent imaging tool for dynamic tracking of $O_2^{\bullet-}$ in live cells and in vivo.

Reactive oxygen species (ROS) are pivotal intermediates as causative agents in many toxicological mechanisms.[1] Abundant evidence suggests that excessively produced ROS can be implicated in a wide variety of diseases, including degenerative disorders[2] and ischemia-reperfusion (IR) injury in surgery.[3] Since superoxide anion ($O_2^{\bullet-}$) is the precursor of other ROS,[4] elucidating the relation between $O_2^{\bullet-}$ fluxes and diseases is of great importance.

One-photon (OP) fluorescence imaging offers a powerful approach to monitor intracellular $O_2^{\bullet-}$ levels owing to its high sensitivity.[5] However, existing $O_2^{\bullet-}$ fluorescent probes used for cell imaging have some drawbacks. For instance, small molecular fluorescent probes often suffer from interference from other ROS,[6] delayed response time,[7] and irreversible reactions.[7] Thus, alternative $O_2^{\bullet-}$ fluorogenic probes with distinct advantages, such as high specificity, instantaneous response, and reversible interaction, remain in urgent demand for bioimaging in cells and in vivo.

As is well known, two-photon (TP) imaging possesses distinct advantages, including increased penetration depth and reduced specimen photodamage, due to its excitation utilizing two lower energy photons.[8] Although several TP probes have been used for imaging thiols,[9] H_2O_2,[10] metal ions,[11] and so on, there has been no report on the TP imaging of $O_2^{\bullet-}$ in live cells or in vivo. For ideal monitoring of $O_2^{\bullet-}$ fluxes, considering the extremely short lifetime and low concentrations of intracellular $O_2^{\bullet-}$, the fluorescent probe must offer greater penetration depth and less photodamage, as well as high sensitivity, instantaneous response, and reversibility. Therefore, it is urgently desired to construct a novel probe combining the merits of OP and TP fluorescence imaging features (we call it dual-mode for short), for dynamically monitoring fluctuations of $O_2^{\bullet-}$ selectively, instantaneously, and reversibly. Furthermore, this dual-mode image not only can improve greatly the accuracy of the $O_2^{\bullet-}$ detection but also can be adopted flexibly according to depths of various samples. As far as we know, no reports to date have been published on the use of dual-mode fluorescent probes to image $O_2^{\bullet-}$.

Inspired by the interaction between caffeic acid phenethyl ester and $O_2^{\bullet-}$,[12] a novel turn-on probe, *N*,*N*′-di-((2*E*)-3-(3,4-dihydroxyphenyl)acrylic acyl)-1,3,5-triazine-2,4,6-triamine (TCA), for $O_2^{\bullet-}$ was designed on the basis of a tripolycyanamide scaffold, covalently conjugating with two caffeic acid molecules (Scheme 1). In the presence of $O_2^{\bullet-}$, we hypothesized that caffeic acid residue of TCA can transform from pyrocatechol, an electron-donor, to benzoquinone (TCAO), an electron-acceptor. By a computational study performed at the B3LYP/6-31G(d,p) level, we confirmed that the charges on caffeic acid moiety of TCAO decreased upon changing hydroxyl to carbonyl (Supporting Information, Figure S1). As expected, a reversible fluorescent probe was obtained. Our results showed that OP and TP fluorescence of TCA were enhanced markedly in the presence of $O_2^{\bullet-}$. Importantly, the probe TCA was successfully applied to hepatocytes, zebrafish, and mice to dynamically visualize the changes in $O_2^{\bullet-}$ levels under various types of stimulation. Those results clearly showed that the TCA has great promise to accurately and dynamically image $O_2^{\bullet-}$ fluctuations in cells and in vivo.

Scheme 1. Structures of TCA and TCAO

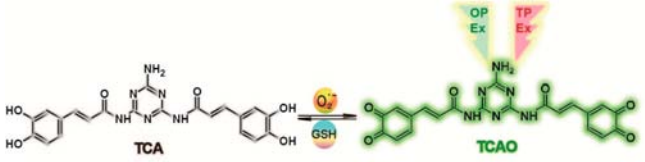

Received: August 17, 2013
Published: September 23, 2013

The photophysical properties of TCA were tested under simulated physiological conditions (Tris buffer, pH 7.4). It emits at around 515 nm and is excited at ~491 nm (OP) and 800 nm (TP). Upon addition of $O_2^{\bullet-}$, the OP fluorescence intensity increased markedly (Figures 1a and S2), as also

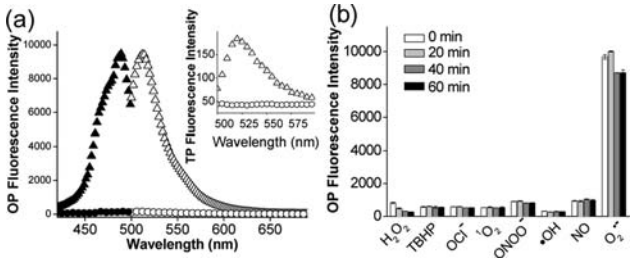

Figure 1. Photophysical properties and selectivity. (a) OP excitation and emission spectra for TCA (10 μM) before (●,○) and after (▲,Δ) addition of $O_2^{\bullet-}$ (20 μM). Inset: TP emission spectra for TCA (10 μM) before (○) and after (Δ) addition of $O_2^{\bullet-}$ (20 μM). All of the spectra were acquired in 0.03 M Tris buffer (pH 7.4) at λ_{ex} = 491 nm (OP) and 800 nm (TP). (b) Fluorescence responses of 10 μM TCA to various reactive oxygen and nitrogen species (20 mM H_2O_2, 200 μM TBHP, 200 μM NaClO, 200 μM $^1O_2$, 33 μM $ONOO^-$, 200 μM $^{\bullet}OH$, 200 μM NO, and 20 μM $O_2^{\bullet-}$). Bars represent the fluorescence 0−60 min after addition of each reactive species. Data were acquired in 0.03 M Tris, pH 7.4, with λ_{ex} = 491 nm.

observed in the TP process (Figure 1a inset). Furthermore, TCA converted into TCAO with a concomitant increase in OP fluorescence which is linear for $O_2^{\bullet-}$concentrations ranging from 1.0×10^{-8} to 2.0×10^{-5} M (Figure S2), and the linear regression equation was $F = 271.0\ O_2^{\bullet-}$ (μM) + 3578, with a correlation coefficient of 0.9950. The detection limit was calculated to be 2.3 nM, as defined by IUPAC based on triplicate measurements of the relative standard. The nature of TCA enables it to quantitatively determine $O_2^{\bullet-}$ with high sensitivity.

The reversibility of the probe was then assessed. The reversible cycles of the probe were mediated by $O_2^{\bullet-}$ or glutathione (GSH). As indicated in Figures S3 and S4, the fluorescence intensity of the probe increased evidently in the presence of $O_2^{\bullet-}$, owing to the proton transfer of pyrocatechol from TCA to $O_2^{\bullet-}$;[14] namely, upon dehydrogenation of TCA, highly fluorescent TCAO formed. Fluorescence then decreased upon addition of GSH as a proton donor for TCAO, due to the rapid formation of low-fluorescent TCA. This reversible cycle can be repeated three times more under the same conditions. The decline of TCAO fluorescence with different concentrations of GSH is shown in Figure S5. The reversibility implies an advantage of TCA for dynamic determination of $O_2^{\bullet-}$ in cells and in vivo.

To prove the selectivity of TCA for $O_2^{\bullet-}$, we studied its responses toward competing ROS,[15,16] reactive nitrogen species (RNS), and metal ions. The results showed that TCA exhibited high selectivity for $O_2^{\bullet-}$ and was unperturbed upon the addition of other ROS, RNS, and metal ions, including hydrogen peroxide (H_2O_2), *tert*-butylhydroperoxide (TBHP), hypochlorite (OCl^-), singlet oxygen ($^1O_2$), peroxynitrite ($ONOO^-$), hydroxyl radical ($^{\bullet}OH$), nitric oxide (NO), Fe^{3+}, Fe^{2+}, Cu^{2+}, Cu^+, and Zn^{2+} (Figures 1b, S6, and S7). TCA displayed an instantaneous response, good photostability, pH insensitivity, and low cytotoxicity (Figures S8−S10). Thus, features of reaction between TCA and intracellular $O_2^{\bullet-}$, including selectivity, reversibility, and instantaneity, make it capable of probing $O_2^{\bullet-}$ dynamically in cells and in vivo.

With a probe in hand that met the need of $O_2^{\bullet-}$ detection in live cells, we attempted to monitor intracellular $O_2^{\bullet-}$ using a dual-mode imaging method. In Figure 2, panels c (OP imaging)

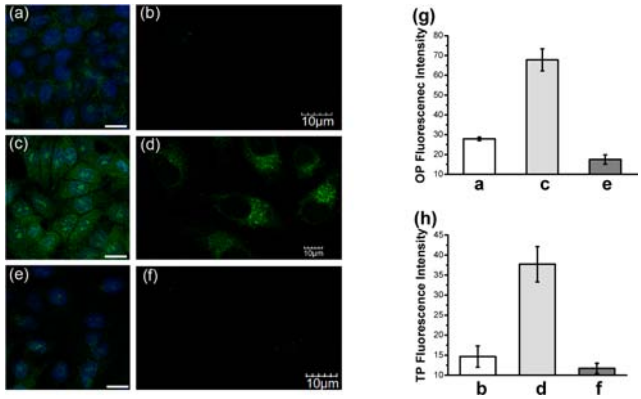

Figure 2. Fluorescence images of $O_2^{\bullet-}$ levels in hepatocytes. One-photon (a,c,e) and two-photon (b,d,f) fluorescence images of HL-7702 cells incubated with 10 μM TCA (green) and 10 μM Hoechst 33342 (the commercial cell nucleolus dye, blue). (c,d) Cells were pretreated with PMA (1.0 μg/mL) for 30 min. (e,f) The PMA-stimulated cells were incubated with 10 μM Tiron for 30 min. One-photon images were acquired using 405 nm (Hoechst 33342) and 488 nm (TCA) excitation, and fluorescence emission windows: blue = 400−470 nm, green = 500−600 nm. Two-photon excitation wavelength was at 770 nm and emission windows 500−550 nm. Scale bar = 15 μm. (g,h) Relative OP and TP fluorescence intensity of TCA-labeled cells in panels a−f. Cells shown are representative images from replicate experiments (n = 5).

and d (TP imaging) indicate that hepatocytes stained with TCA fluoresced strongly after being treated with phorbol-12-myristate-13-acetate (PMA), enhancing $O_2^{\bullet-}$ release in cells.[15,16] In contrast, upon the addition of superoxide scavenger (Tiron), fluorescence intensity weakened distinctly (Figure 2e,f), which was consistent with the results of superoxide dismutases and Tiron scavenger experiments in cellular extracts (Figure S11). Moreover, identical results from OP and TP imaging indicated that TCA could dynamically visualize the changes of $O_2^{\bullet-}$ levels in hepatocytes. Additionally, OP images present a wider field to facilitate parallel analysis;[17] meanwhile, TP images express higher signal-to-noise ratio because of minimal interference from background autofluorescence. More importantly, this dual-mode method makes the results more convincing.

Previous reports suggested that liver injury mediated by IR is the major cause of morbidity and mortality in liver surgery and transplantation.[18] The mechanisms of IR injury are most relevant to ROS.[2] In the existing studies, ROS produced from Kupffer cells and neutrophils can at least partially diffuse into hepatocytes and induce cell injury under IR conditions.[19] However, up to now, it has been a challenge to demonstrate that IR-induced ROS are overgenerated in the hepatocytes, which make up 85% of the liver.[20,21] Given that $O_2^{\bullet-}$ is the first oxygen-derived free radical and can trigger generation of other ROS, it is crucial to explore carefully $O_2^{\bullet-}$ fluctuations in hepatocytes during IR injury. Here, we used an oxygen and glucose deprivation (OGD) reperfusion mdel[22] to imitate IR conditions with the aim to gain insight into the relationship between $O_2^{\bullet-}$ fluctuations and IR injury inside hepatocytes.

dx.doi.org/10.1021/ja408524j | J. Am. Chem. Soc. 2013, 135, 14956−14959

Dual-mode images (Figure 3a,b) indicated that hepatocytes exhibited weak fluorescence under OGD conditions. Subsequently, both high sensitivity of OP (Figure 3c) and high temporal/spatial resolution of TP (Figure 3d) images showed that $O_2^{\bullet-}$ increased notably after reperfusion. These results signified that $O_2^{\bullet-}$ played a vital role in liver reperfusion injury. Besides, we speculated that the main source of the overproduction of $O_2^{\bullet-}$ in hepatocytes under OGD reperfusion was mitochondrial respiratory chain complex II (Figures S12 and S13).

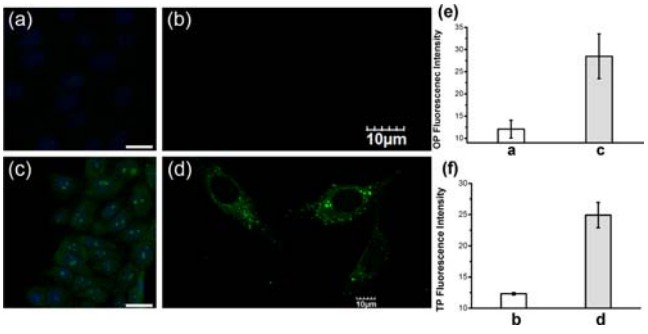

Figure 3. Fluorescence images of $O_2^{\bullet-}$ levels in hepatocytes before and after reperfusion. One-photon (a,c) and two-photon (b,d) fluorescence images of HL-7702 cells incubated with 10 μM TCA (green) and 10 μM Hoechst 33342 (blue). (a,b) Cells were pretreated with 5 mM sodium hydrosulfite (an oxygen-free medium) in glucose-free DMEM for 30 min. (c,d) Pretreated cells were reperfused with high-glucose DMEM for 30 min, and in the absence of sodium hydrosulfide. Images were acquired using 405 and 488 nm for OP excitation, and 770 nm for TP excitation. OP fluorescence emission windows: blue = 400−470 nm, green = 500−600 nm. TP fluorescence emission windows: 500−550 nm. Scale bar = 15 μm. (e,f) Relative OP and TP fluorescence intensity of TCA-labeled cells in panels a−d. Cells shown are representative images from replicate experiments (n = 5).

To test the reversibility of TCA fluorescence in live cells, OP fluorescence imaging of reversible cycles in hepatocytes was then undertaken. A bright fluorescence was definitely observed when the probe-loaded cells were incubated with PMA for 30 min (Figure 4b). The fluorescence of these cells then decreased markedly after addition of GSH (Figure 4c). Another reversible cycle can be easily achieved by again adding PMA and GSH (Figure 4d,e). These results strongly suggest that TCA has reversibility to image $O_2^{\bullet-}$ levels in living cells.

Next we assess the dynamic fluorescence responses of TCA to real-time changes of $O_2^{\bullet-}$ levels in the process of cell apoptosis, referring to previous reports that $O_2^{\bullet-}$ is increased in cells exposed to an apoptotic stimulus.[23] Consistent with previous findings, OP fluorescence images clearly show that TCA fluorescence is progressively enhanced with prolonged time in liver cancer cells preincubated with L-buthionine sulfoximine (BSO) (Figure 5a), indicating dramatically increased $O_2^{\bullet-}$ concentrations. Meanwhile, upon BSO treatment, the cells showed morphological features, i.e., shrinkage and budding. After BSO was removed, the fluorescence intensity declined gradually in these cells, indicating that intracellular GSH increased in the absence of BSO, which also rescues the cells from apoptosis.[24] The dynamic changes in $O_2^{\bullet-}$ levels after the cells were stimulated by PMA are shown in Figure S14. The results imply that TCA is an ideal imaging tool to dynamically and reversibly monitor intracellular $O_2^{\bullet-}$ levels.

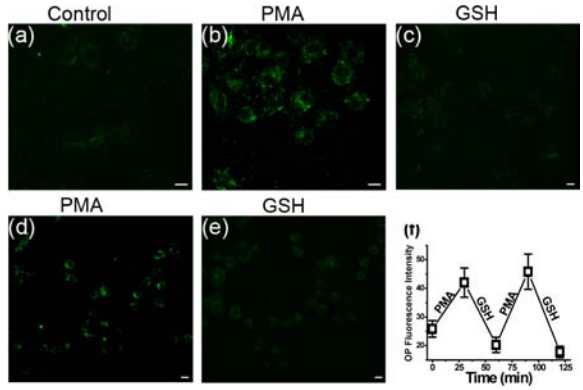

Figure 4. OP fluorescence imaging of reversible cycles in hepatocytes. (a) Cells loaded with 10 μM TCA for 30 min. (b) Probe-loaded cells treated with PMA (1.0 μg/mL) for 30 min. (c) Probe-loaded, PMA-treated cells incubated with GSH (2 mM) for 30 min. (d) The cells above exposed to a second dose of PMA (1.0 μg/mL) for an additional 30 min. (e) The cells above exposed to a second dose of GSH (2 mM) for an additional 30 min. (f) Relative OP fluorescence intensity of TCA-labeled cells in panels a−e. Cells shown are representative images from replicate experiments (n = 5). Scale bar = 15 μm.

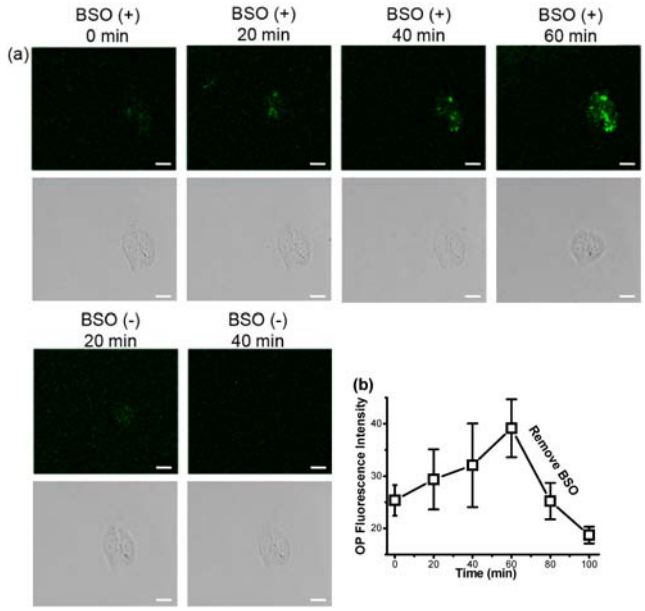

Figure 5. Real-time fluorescence imaging during BSO-induced apoptosis. (a) 10 μM TCA-loaded HepG2 cells were treated with 5 mM BSO (0, 20, 40, and 60 min). BSO was then removed, and the cells were further cultured in a fresh cell medium (20 and 40 min). (b) Relative OP fluorescence intensity of TCA-labeled cells in panel a. Cells shown are representative images from replicate experiments (n = 5). Scale bar = 15 μm.

To validate the applications of TCA in intra-vital imaging, the probe was used to detect changes in $O_2^{\bullet-}$ levels deep inside live zebrafish (Figure S15). The dual-mode approach provides large visual fields (OP) and distinct images (TP) of $O_2^{\bullet-}$ fluctuations in zebrafish reperfusion injury.

In vivo imaging was next successfully realized in mice with liver IR. In situ TP images were acquired from simulated liver surgery (Figure 6). The injured liver emitted bright fluorescence after IR compared with the control (Figure 6b). These results indicated that $O_2^{\bullet-}$ was overgenerated after simulated liver surgery, and IR injury was mediated directly by

dx.doi.org/10.1021/ja408524j | J. Am. Chem. Soc. 2013, 135, 14956−14959

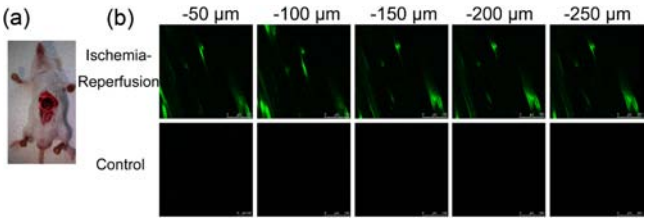

Figure 6. Changes in $O_2^{\bullet-}$ levels in mice with liver IR. (a) The surgical procedure exposes the left liver lobe for imaging. (b) TP fluorescence in situ images of liver with TCA (100 μM). Images were acquired using 770 nm TP excitation. TP fluorescence emission windows: 500–550 nm Scale bar = 100 μm.

$O_2^{\bullet-}$. With the advantage of TP deep-tissue imaging (250 μm), broader applications of TCA can be achieved in bioimaging.

In summary, a novel $O_2^{\bullet-}$ probe combining the merits of one-photon and two-photon fluorescence properties has been synthesized and applied for dynamic monitoring of $O_2^{\bullet-}$ fluxes selectively, instantaneously, and reversibly. The probe can dynamically and reversibly respond to intracellular $O_2^{\bullet-}$ under apoptotic stimuli. With good sensitivity, wide field of OP imaging, and high resolution and deep tissue penetration of TP imaging, the probe is well-suited as a dual-mode fluorescent imaging tool for tracking $O_2^{\bullet-}$ fluctuations in hepatocytes, zebrafish, and mice during mimicked IR injury, which revealed that overproduction of $O_2^{\bullet-}$ is closely related to reperfusion injury. The outstanding features of the probe, which can be easily used at various depths for imaging of $O_2^{\bullet-}$, make it an ideal tool for dynamic and reversible investigation of $O_2^{\bullet-}$ fluctuations in live cells and in vivo.

■ ASSOCIATED CONTENT

Ⓢ Supporting Information

Synthesis, characterization, and experimental details. This material is available free of charge via the Internet at http://pubs.acs.org.

■ AUTHOR INFORMATION

Corresponding Author

tangb@sdnu.edu.cn

Author Contributions

†Wen Zhang and Ping Li contributed equally.

Notes

The authors declare no competing financial interest.

■ ACKNOWLEDGMENTS

This work was supported by 973 Program (2013CB933800), National Natural Science Foundation of China (21227005, 21035003, and 21205073), Specialized Research Fund for the Doctoral Program of Higher Education of China (20113704130001), and Program for Changjiang Scholars and Innovative Research Team in University and Science and Technology Development Programs of Shandong Province of China (2010G0020243).

■ REFERENCES

(1) Halliwell, B.; Gutteridge, J. M. *Biochem. J.* **1984**, *219*, 1–14.
(2) Wallace, D. C. *Science* **1999**, *283*, 1482–1488.
(3) McCord, J. M. *N. Engl. J. Med.* **1985**, *312*, 159–163.
(4) Dickinson, B. C.; Chang, C. J. *Nat. Chem. Biol.* **2011**, *7*, 504–511.
(5) Stephens, D. J.; Allan, V. J. *Science* **2003**, *300*, 82–86.
(6) Murphy, M. P.; Holmgren, A.; Larsson, N.; Halliwell, B.; Chang, C. J.; Kalyanaraman, B.; Rhee, S. G.; Thornalley, P. J.; Partridge, L.; Gems, D.; Nyström, T.; Belousov, V.; Schumacker, P. T.; Winterbourn, C. C. *Cell. Metab.* **2011**, *13*, 361–366.
(7) Gao, J. J.; Xu, K. H.; Tang, B.; Yin, L. L.; Yang, G. W.; An, L. G. *FEBS J.* **2007**, *274*, 1725–1733.
(8) Denk, W.; Strickler, J. H.; Webb, W. W. *Science* **1990**, *248*, 73–76.
(9) Lee, J. H.; Lim, C.; S. Tian, Y. S.; Han, J. H.; Cho, B. R. *J. Am. Chem. Soc.* **2010**, *132*, 1216–1217.
(10) Chung, C.; Srikun, D.; Lim, C. S.; Chang, C. J.; Cho, B. R. *Chem. Commun.* **2011**, *47*, 9618–9620.
(11) Masanta, G.; Lim, C. S.; Kim, H. J.; Han, J. H.; Kim, H. M.; Cho, B. R. *J. Am. Chem. Soc.* **2011**, *133*, 5698–5700.
(12) Chen, J. H.; Ho, C. T. *J. Agric. Food Chem.* **1997**, *45*, 2374–2378.
(13) Yuan, L.; Lin, W.; Zhao, S.; Gao, W.; Chen, B.; He, L.; Zhu, S. *J. Am. Chem. Soc.* **2012**, *134*, 13510–13523.
(14) Sawyer, D. T.; Gibian, M. J.; Morrison, M. M.; Seo, E. T. *J. Am. Chem. Soc.* **1978**, *100*, 627–628.
(15) Maeda, H.; Yamamoto, K.; Nomura, Y.; Kohno, I.; Hafsi, L.; Ueda, N.; Yoshida, S.; Fukuda, M.; Fukuyasu, Y.; Yamauchi, Y.; Itoh, N. *J. Am. Chem. Soc.* **2005**, *127*, 68–69.
(16) Oushiki, D.; Kojima, H.; Terai, T.; Arita, M.; Hanaoka, K.; Urano, Y.; Nagano, T. *J. Am. Chem. Soc.* **2010**, *132*, 2795–2801.
(17) Oheim, M.; Michael, D. J.; Geisbauer, M.; Madsen, D.; Chow, R. H. *Adv. Drug Delivery Rev.* **2006**, *58*, 788–808.
(18) Kohli, V.; Selzner, M.; Madden, J. F.; Bentley, R. C.; Clavien, P. A. *Transplantation* **1999**, *67*, 1099–1105.
(19) Jaeschke, H. *Hepatology* **2002**, *36*, 761–763.
(20) Michael, M. D.; Kulkarni, R. N.; Postic, C.; Previs, S. F.; Shulman, G. I.; Magnuson, M. A.; Kahn, C. R. *Mol. Cell* **2000**, *6*, 87–97.
(21) Decaens, C.; Durand, M.; Grosse, B.; Cassio, D. *Biol. Cell.* **2008**, *100*, 387–398.
(22) Rytter, A.; Cronberg, T.; Asztély, F.; Nemali, S.; Wieloch, T. *J. Cereb. Blood Flow. Metab.* **2003**, *23*, 23–33.
(23) Douglas, R. G.; John, C. R. *Science* **1998**, *281*, 1309–1312.
(24) Xu, K.; Qiang, M.; Gao, W.; Su, R.; Li, N.; Gao, Y.; Xie, Y.; Kong, F.; Tang, B. *Chem. Sci.* **2013**, *4*, 1079–1086.